

# Medical imaging by NMR

By P. Mansfield, B.Sc., Ph.D., and A. A. Maudsley B.Sc., Ph.D.

Department of Physics, University of Nottingham

(Received June, 1976 and in revised form November, 1976)

## ABSTRACT

Application of the new nuclear magnetic resonance (NMR) method of fast scan proton imaging is described. Cross sectional proton scans of a human finger *in vivo* are measured and reveal considerable anatomical detail, particularly of the soft tissue regions. Imaging of tumour tissue is also briefly discussed.

During the past few years new techniques have been developed in nuclear magnetic resonance (NMR) which make it possible to form two dimensional cross-sectional images related to the distribution of protons in biological structures (Hinshaw, 1974a&b, 1976; Kumar *et al.*, 1975; Lauterbur, 1973, 1974; Mansfield and Grannell, 1973, 1975a). The methods are non-invasive and of low radiation hazard and could therefore have some clinical value in medical diagnosis. The first crude medical picture of a human finger taken *in vivo* (Mansfield *et al.*, 1974; see also Mansfield and Grannell, 1975b) relied on a slow and inexact imaging method based on reconstruction from a number of projection absorption profiles. Only the gross outline with no internal detail was revealed.

Recently we introduced a new imaging technique which does not depend on reconstruction from projections (Garroway *et al.*, 1974). It relies on selective irradiation of the specimen in switched magnetic field gradients. In the fast scan adaptation of this method (Mansfield *et al.*, 1976) the mobile proton spin density is obtained directly, line by line across the specimen cross-section. Since this work, the apparatus and display have been considerably improved (Baines and Mansfield, 1976) thus enabling us to produce reasonably detailed pictures of a human specimen *in vivo*.

In this paper we wish to report new results obtained with live fingers, particularly with reference to the anatomical information obtained by NMR imaging in normal tissue. Brief reference will be made to imaging of tumour tissue, though we hope to present a more detailed discussion of this aspect of imaging elsewhere.

## Principle of operation

The study of structure in materials cannot ordinarily be attempted with conventional NMR techniques. This is because NMR measures frequency differences or magnetic field variations and

each piece of resonant material in a specimen is not uniquely defined magnetically. However, by using a combination of switched linear magnetic field gradients plus selective irradiation of the sample, it is possible to uniquely assign a frequency to a particular point in the specimen. The NMR signal coming from a localized region of the sample is directly related to the mobile proton density at that point. By mobile protons we have in mind those contained in the free or nearly free water, fat or oil distributed throughout the soft tissue regions of the specimen. Bone structures, therefore, which contain relatively few mobile protons, are generally detectable through their lack of signal, while tumours and other soft tissues give strong signals. This behaviour contrasts with that of conventional X-rays which are scattered only rather weakly by protons and so usually give pictures for soft tissue regions with relatively poor definition.

## METHOD

The specimen is placed in a large static magnetic field  $B$  which polarizes all nuclear spins. (Since biological tissue contains 75-80% by weight of water we are particularly interested in the proton spin

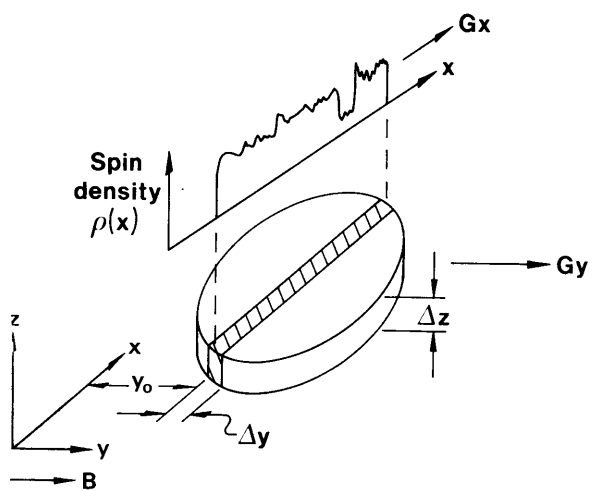


FIG. 1.

Sketch illustrating the principle of line scanning by selectively irradiating a magnet strip within an isolated slice of magnetization.

## Medical imaging by NMR

magnetization, though one could with less sensitivity observe other nuclei.) In addition to this field, switched linear magnetic field gradients are applied along two (or three) principal coordinate axes. We first consider a thin disc or slice of magnetization of thickness  $\Delta z$  within the specimen. Such a slice is sketched in Fig. 1 and is, of course, part of an extended specimen along the  $z$  axis.

The field gradient  $G_y$  alone is switched on and the spins within the narrow strip  $\Delta y$  at  $y_0$  are selectively excited by applying a "tailored" r.f. pulse to the specimen. The tailoring of the pulse consists of shaping the r.f. envelope such that its spectral distribution is confined to a narrow band of frequencies. A square unshaped pulse, by contrast, has a sinc function frequency spectrum with a width characterized by the inverse pulse length but with extensive sidebands. The r.f. components of the tailored pulse interact with spins in a narrow strip (shaded strip of Fig. 1). This interaction is brought about because the spins within the disc of material have a range of nuclear Larmor frequencies through the action of the linear magnetic field gradient  $G_y$ .

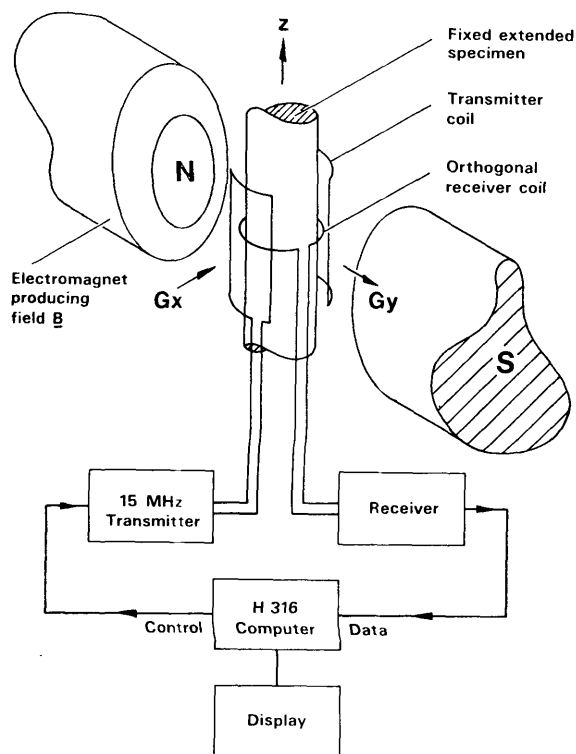


FIG. 2.

Simplified representation of the 15 MHz NMR imaging apparatus. The field gradient coils producing  $G_x$  and  $G_y$  are not shown.

Thus only those spins within the shaded strip, which have the right Larmor resonance frequency, can respond to the selective r.f. pulse.

Immediately following this selective excitation pulse, the field gradient is switched from  $G_y$  to  $G_x$  and the spin response or free induction decay (FID) signal is recorded and Fourier transformed. For a narrow strip ( $\Delta y$  small) at position  $y_0$  in either a thin slice ( $\Delta z$  small), or for a sample with cylindrical symmetry, this Fourier transformed signal is directly proportional to the proton spin density  $\rho(x, y_0)$  along  $x$ . The transformed signals for each strip of the specimen are used to modulate the spot intensity of an oscilloscope in a television raster display to form a cross-sectional picture of the object. The display employs a 16-level linear grey scale covering the intensity range black for zero signal to white for high spin density (Baines and Mansfield, 1976).

The initial specialization to a layer or plane can itself be achieved by a selective irradiation procedure in a third field gradient  $G_z$ . In these experiments, however, specialization to a layer is achieved simply by relying on the receiver coil geometry. This is a flat coil of 2 cm diameter and our experiments show that most of the received signal comes from a layer approximately 8 mm thick.

A simplified diagram of the imaging apparatus is shown in Fig. 2. The 15 MHz r.f. excitation pulses



FIG. 3.

Cross-sectional proton scan of a phantom filled with mineral oil (see text for details). The time to produce this picture was 40.5 min. The full picture size slightly exceeds a  $64 \times 64$  data array, thus squaring off the circular edges. The missing data were not lost but overflowed into the other quadrants of a  $128 \times 128$  data array. The field gradients were  $G_x = 0.69 \text{ G cm}^{-1}$  and  $G_y = 0.86 \text{ G cm}^{-1}$ . Each line of the picture was averaged 128 times.

are fed from the transmitter to a pair of cylindrical Helmholtz coils (Ginsberg and Melchner, 1970) surrounding the sample as shown. The peak pulse power was 1.0 watt and the pulse duration 7.4 msec. The production and shaping of the pulses, switching of the field gradients, data acquisition, Fourier transformation and data display are all performed on-line with a Honeywell H316 minicomputer. A more detailed description of the apparatus and the method is given by Mansfield *et al.* (1976). Placing the finger in the receiver coil was found to increase the received noise through the antenna action of the body. However, we found that simply holding an earthed sheet with the free hand reduced the pick up. No other special precautions were taken to shield the receiver coil against induced noise.

## RESULTS

### *Phantom test*

Figure 3 is a cross-sectional picture of the proton distribution of mineral oil in a phantom object and illustrates the spatial resolution obtainable in the present line-scan imaging experiments. The sample consisted of a thick-walled 1.4 mm bore glass capillary tube and a solid circular glass rod immersed in mineral oil, the whole being contained in a circular cross-section glass test-tube of inside diameter 14.6 mm. This picture and all biological pictures presented in the next sections are made up from  $64 \times 64$  point arrays.

A linear grey scale wedge is added to later pictures to aid intensity comparisons; however, for precise measurements actual data can be output numerically.

### *Spin-lattice relaxation effects*

We assume here that the local spin magnetization at coordinates  $x, y$  in a given plane  $z$  is destroyed following one selective excitation pulse, but recovers exponentially, through a single simple spin-lattice relaxation process in a characteristic time  $T_1(xy)$ . Thus the effective spin density  $\rho(xy\tau)$  observed in these images depends on the time delay  $\tau$  between successive excitation pulses according to the relationship  $\rho(xy\tau) = \rho(xy)[1 - e^{-\tau/T_1(xy)}]$ . That is to say, it is possible for localized regions of the specimen to give a picture brightness which is less than the localized spin density would suggest; for example, if the ratio  $\tau/T_1(xy)$  is small. We refer to this effect as spin-lattice relaxation time discrimination and most of the intensity variations between tissue types seem to be attributable to this effect rather than to real density variations, though if present, these too will aid picture contrast.

The variations in  $T_1(xy)$  within a specimen are a reflection of the variations of both the mobility of the free water, fat or oil and the concentration of dissolved minerals, nutrients, etc., characteristic of the various tissues.

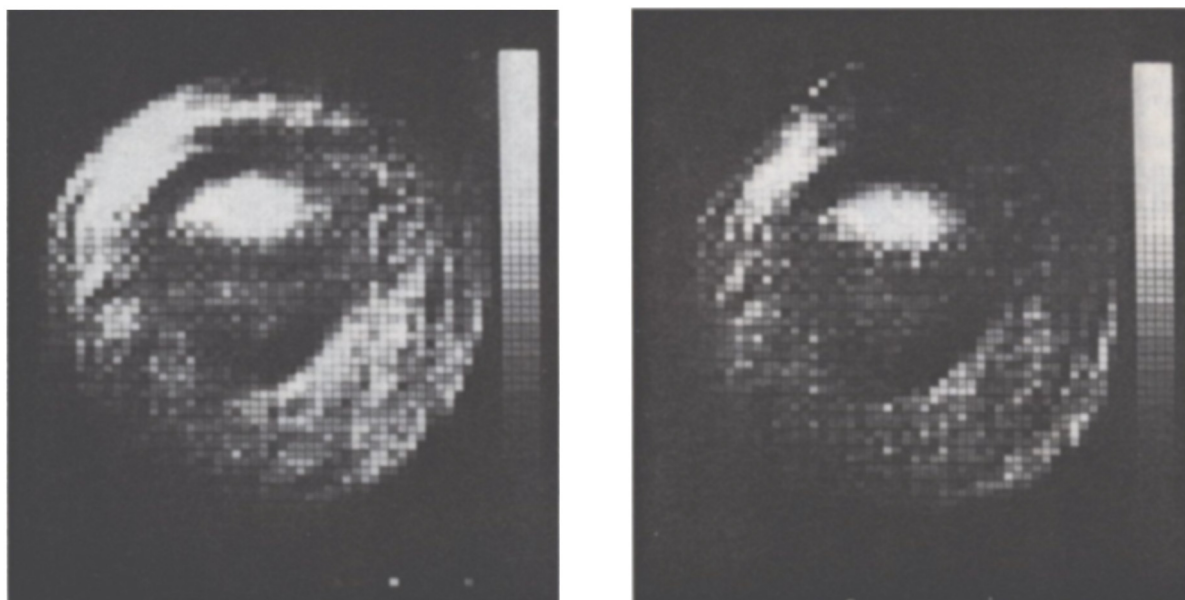
### *Finger images recorded in vivo.*

A number of cross-sectional proton scans have been produced at various positions along the right hand third digit of AAM. We have found that quite good discrimination between the various tissues can be obtained using a delay of 0.5 sec. Similar results and discrimination were found with the finger of another subject (PM).

Two scans midway along the mid-phalanx of AAM's third right hand digit are shown in Fig. 4 and correspond to cross-sectional views looking into the end of the digit. The dorsal plane passes through the top and the palmar plane through the bottom of each picture. The delay in Fig. 4A was 0.5 sec. Each line of this picture was averaged 48 times. The final picture took 23 mins to produce. Figure 4B is a proton scan of the same cross-section as 4A, but with the delay  $\tau$  reduced to 0.3 sec. This picture took 15 min. to produce. The irradiation gradient  $G_y$  was  $0.41 G \text{ cm}^{-1}$  and the read gradient  $G_x$  was  $0.34 G \text{ cm}^{-1}$  for both pictures. Figures 5A and B are colour representations of the data of Figs. 4A and B. The data are presented through a window comprising eight distinguishable colours corresponding to eight out of the original 16 data levels. In order to give easier discrimination the window base level and the colour scales were set in each case to maximize colour contrast between data levels. Figure 6 is a sketch traced off Fig. 4A showing more clearly the anatomical details that we have been able to recognize (Kaplan, 1965; Landsmeer, 1976). (Inevitably some clarity is lost from these pictures in the photographic reproduction.)

Strong signals are received from the skin and subcutaneous areolar and fibro-fatty tissue giving the general outline of the mid-phalangeal cross-section. The bone tissue shows as a dark ring surrounding the bright zone produced by strong signals from the marrow region. Immediately below the bone is a second dark ring structure of the fibrous flexor tendon sheath. Within this and slightly brighter are the central flexor profundus and the two unresolved components of the flexor sublimis tendons (flexor digitorum superficialis). Above the bone towards the dorsal plane is a dark horizontal line corresponding to the unresolved mid- and lateral bands of the mid-phalanx extensor tendons. Figures 4B and 5B show the same general characteristics as 4A and 5A, but the

## Medical imaging by NMR



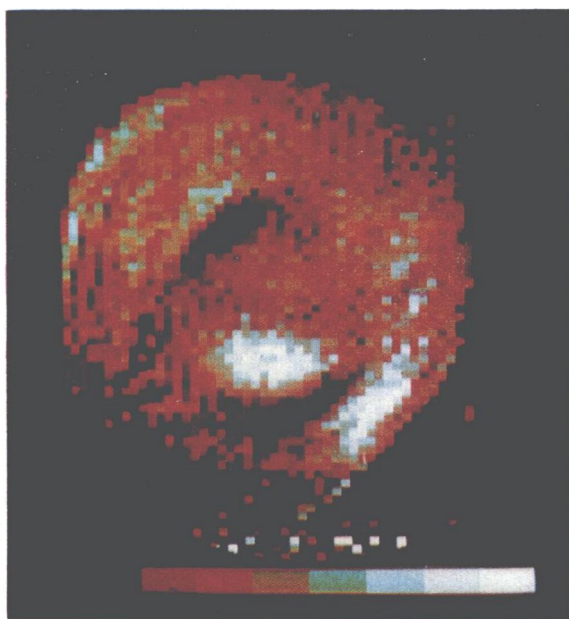
10 mm

A

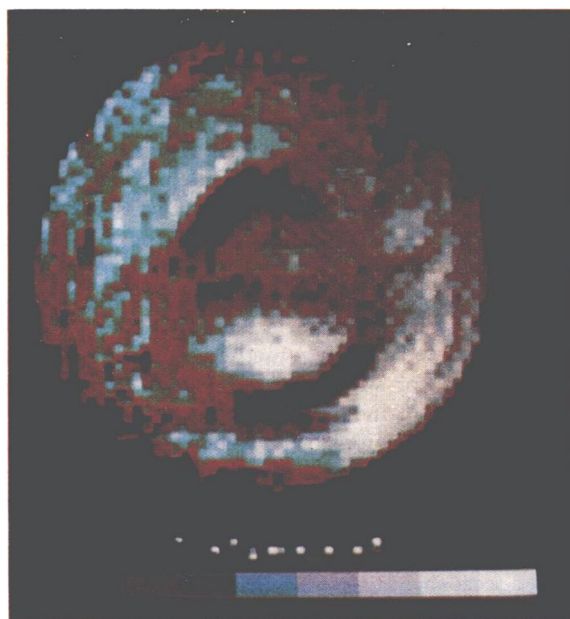
FIG. 4.

B

Cross-sectional images of a finger obtained *in vivo* by NMR (see text for full details).  
 (A) delay  $\tau=0.5$  sec. (B) delay  $\tau=0.3$  sec.



A



B

FIG. 5.

Colour versions of the finger images shown in Figs. 4A and B.  
 (A) The eight colours black through to white correspond to data levels 6-13. The delay time  $\tau=0.5$  sec.  
 (B) The eight colours black through to white correspond to data levels 2-9.  
 In both pictures, data falling outside the window limits are presented as all black or all white as appropriate.

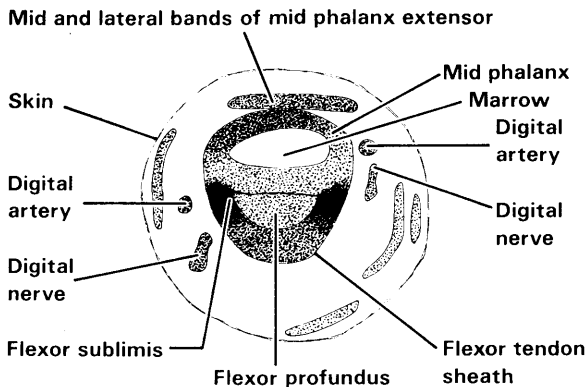


FIG. 6.

A reduced tracing from Fig. 4A showing the recognizable anatomical detail that we have been able to obtain from it.

overall brightness and level of discrimination of the black and white image is reduced with the shorter delay. Differentiation of the flexor profundus from the periosteum and chiasma tendinum are less pronounced indicating that the  $T_1$  of the flexor profundus is of the order of 0.3 sec. The marrow region, on the other hand, remains quite bright. This suggests a  $T_1$  much less than 0.3 sec.

The digital arteries and nerves are just resolved in Figs. 4A and 5A and their positions sketched in Fig. 6. The fact that one can distinguish the arteries from the surrounding tissue means that, with higher resolution or with larger blood vessels in other parts of the anatomy, NMR imaging offers the possibility of making direct blood flow measurements. The principle of such measurements depends on the replenishment of spin saturated blood caused by flow of fresh polarized (unsaturated) blood into the sample coil region, thus producing an apparent reduction in the spin-lattice relaxation time of the blood directly related to its flow rate. Slight modifications to the imaging method described would be necessary for such measurements.

Also apparent in these pictures are darker sliver-like concentric regions or pockets as indicated in the sketch. We ascribe these to discontinuous regions

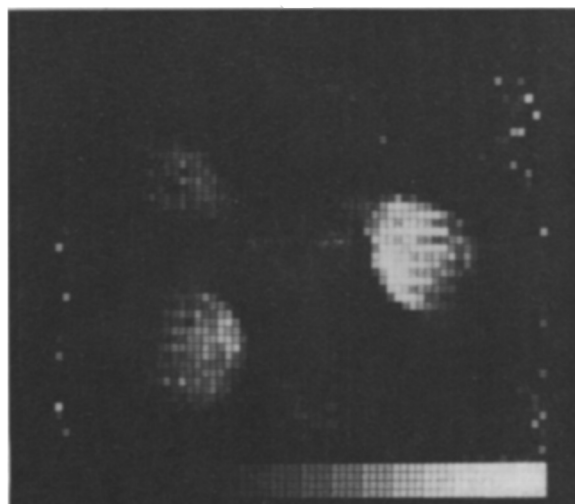
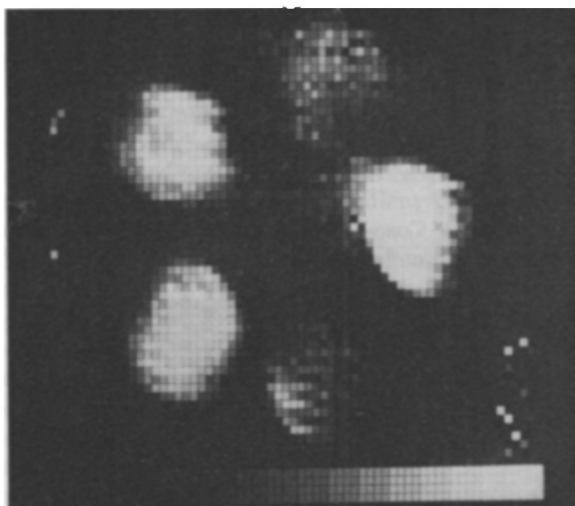
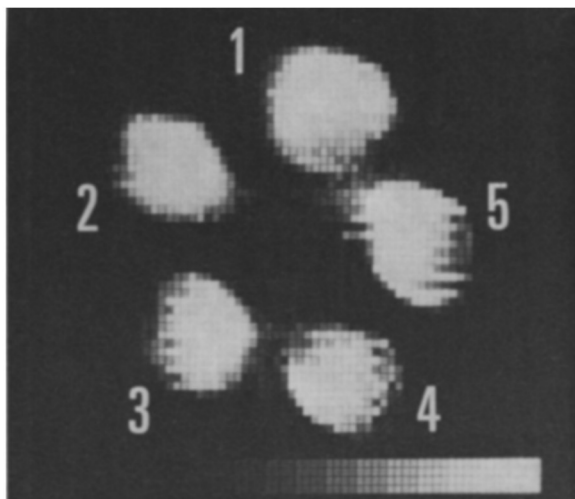


FIG. 7.

Proton scans showing spin-lattice relaxation time discrimination of images obtained from excised rat specimens of normal and malignant tissue. The tissue was contained in 3 mm glass tubes labelled as follows: 1. hepatoma (D23); 2. normal skin tissue; 3. liver; 4. sarcoma (MC7); 5. water control. The specimens in each picture are the same but the delay time  $\tau$  was varied: (A)  $\tau=1.2$  sec; (B)  $\tau=0.67$  sec; (C)  $\tau=0.37$  sec.

*Medical imaging by NMR*

within the fibro-fatty layer which could be either variation in fibro-fatty content or branches of digital nerves or blood vessels. Adipose layers are likely to have a shorter  $T_1$  (Hollis *et al.*, 1975) and would thus appear as bright regions. It would seem from Fig. 4b that these regions, as with other parts of the finger, owe their contrast in the NMR image principally to localized  $T_1$  variations rather than to significant spin density variations.

Cross-sectional scans have also been made through the distal phalangeal joint and the mid point and tip of the distal phalanx. In all cases the general features as reported here are reproduced, though the distal flexor and extensor tendons are more diffuse at the joint and the bone somewhat smaller in the distal region as expected.

## TISSUE TYPES

From the point of view of the present NMR imaging studies, tissue types can be classified by their mobile proton density (in many cases this is essentially the free water content) and spin lattice relaxation time  $T_1$  (see for example Kiricuta and Simplaceanu, 1975; Hollis *et al.*, 1975). If  $T_1$  is similar between two tissue types, one must rely on more accurate measurement of water concentration to differentiate between them. Our measurements are accurate to only one part in 16 (the display range). Lack of computer core has forced us to discard the original information which had an accuracy of 1 in  $10^3$ . Nevertheless, through  $T_1$  differences, striking contrast can be achieved.

Figures 7A-C show a series of NMR images for decreasing delay  $\tau$  obtained from the same set of excised tissue specimens taken from young normal white wistar rats. The samples were contained in four 3 mm i.d. glass tubes, labelled 1-4 in Fig. 7. As a control the fifth tube, number 5, contained doped water with  $T_1 \approx 100$  msec. Tubes 1-4 contained respectively hepatoma (D23), a sample of normal skin tissue, normal liver and sarcoma (MC7). Samples 2-4 were taken from the same animal. Both animals were injected with 0.5 ml of the anti-coagulant heparin. The NMR images were produced within 2 hours of sacrifice. The delay in Fig. 7A was 1.2 sec resulting in no noticeable discrimination between the various specimens. In Fig. 7B, the delay was reduced to 0.67 sec and clear differentiation between the normal and malignant tissues results. The numerical data for this picture show a slight discrimination between the two normal specimens, numbers 2 and 3, and between the two malignant specimens, numbers 1 and 4. Further reduction of the delay time in Fig. 7C reduces the tumour images

to almost zero intensity and begins to affect the intensity of the normal tissue images too. According to Damadian (1971) and others (Weissman *et al.*, 1972; Frey *et al.*, 1972),  $T_1$  in malignant tissue is about 1.5 times longer than that of the corresponding normal tissue. In spite of this small factor, strong intensity contrast is possible in our images by adjusting the delay time  $\tau$ .

## CONCLUSION

We have demonstrated that NMR imaging of fingers *in vivo* is able to produce reasonably clear cross-sectional anatomical pictures in times up to 23 min. No special precautions were taken to clamp the subjects' hand so that blood flow and general movement, at one time considered to be a possible limit to spatial resolution, have not been found to be troublesome. By implication, therefore, we do not anticipate problems in producing cross-sectional images of the limbs and head where movement can be made negligible. Involuntary movements in other parts of the anatomy are likely to be troublesome, however, unless the scan time can be considerably reduced below 23 min. The experiments described produced no sensation in the finger and the mean r.f. power levels used were well below any perceptible heating level.

The results on normal and malignant tissue suggest that tumourous regions of a subject will give good image contrast against a background of normal tissue. This should aid the detection and diagnosis of tumours in cases where there are no obvious geometrical distortions, that is to say in the early detection of cancer.

Our magnet system has restricted the maximum specimen size to a diameter of 2.0 cm. However, we are planning shortly to study much larger specimens at operating frequencies in the range 1-2 MHz using a specially designed low field spherical electro-magnet which is under construction.

## ACKNOWLEDGMENTS

We wish to thank Dr. M. R. Price for supplying the rat tissue specimens and Dr. H. Clow, Mr. P. Walters and the Directorate of the Central Research Laboratories of EMI for producing the colour pictures of our data.

We are also grateful to Professor R. E. Coupland for his helpful comments on the manuscript.

## REFERENCES

- BAINES, T., and MANSFIELD, P., 1977. An improved picture display for NMR imaging. *Journal of Physics E. Scientific Instruments* (in press).  
 DAMADIAN, R., 1971. Tumour Detection by Nuclear Magnetic Resonance, *Science N. Y.*, **171**, 1151-1153.  
 FREY, H. E., KNISPEN, R. R., KRUV, J., SHARP, A. R., THOMPSON, R. T., and PINTAR, M. M., 1972. Proton

- spin-lattice relaxation studies of non-malignant tissues of tumorous mice. *Journal of the National Cancer Institute*, *49*, 903-906.
- GARROWAY, A. N., GRANNEL, P. K., and MANSFIELD, P., 1974. Image formation in NMR by a selective irradiative process. *Journal of Physics, C. Solid State Physics*, *7*, L457-L461.
- GINSBERG, D. M., and MELCHNER, M. J., 1970. Optimum geometry of saddle shaped coils for generating a uniform magnetic field. *The Review of Scientific Instruments*, *41*, 122-123.
- HINSHAW, W. S., 1974a. Spin mapping: the application of moving gradients to NMR. *Physics Letters*, *48A*, 87-88.
- 1974b. The application of time dependent field gradients to NMR spin mapping. *Proceedings of the 18th Congress Ampere*, *2*, 433-434.
1976. Image formation by nuclear magnetic resonance; the sensitive point method. *Journal of Applied Physics*, *47*, 3709-3721.
- HOLLIS, P. H., LEON, A. S., EGGLESTON, J. C., and MORRIS, H. P., 1975. Nuclear magnetic resonance studies of cancer. *Journal of The National Cancer Institute*, *54*, 1469-1472.
- KAPLAN, E. B., 1965. *A Functional and Surgical Anatomy of the hand* (J. B. Lippincott Co., Philadelphia).
- KIRICUTA, I. C., and SIMPLACEANU, V., 1975. Tissue water content and nuclear magnetic resonance in normal and tumour tissue. *Cancer Research*, *35*, 1164-1167.
- KUMAR, A., WELTI, D., and ERNST, R. R., 1975. NMR Fourier zeugmatography. *Journal of Magnetic Resonance*, *18*, 69-83.
- LANDSMEER, J. M. F., 1976. *Atlas of Anatomy of the Hand*: (Churchill Livingstone, London).
- LAUTERBUR, P. C., 1973. Image formation by induced local interactions: examples employing nuclear magnetic resonance. *Nature*, *242*, 190-191.
1974. Magnetic resonance zeugmatography. *Pure and Applied Chemistry*, *40*, 149-157.
- MANSFIELD, P., and GRANNEL, P. K., 1973. NMR diffraction in solids? *Journal of Physics C, Solid State Physics*, *6*, L422-L426.
- 1975a. Diffraction and microscopy in solids and liquids by NMR. *Physical Review B*, *12*, 3618-3634.
- 1975b. Microscopy *in vivo* by nuclear magnetic resonance. *Physics in Medicine and Biology*, *20*, 477-482.
- MANSFIELD, P., GRANNEL, P. K., and MAUDSLEY, A. A., 1974. Diffraction and microscopy in solids and liquids by NMR. *Proceedings of the 18th Congress Ampere*, *2*, 431-432.
- MANSFIELD, P., MAUDSLEY, A. A., and BAINES, T., 1976. Fast scan proton density imaging by NMR. *Journal of Physics E, Scientific Instruments*, *9*, 271-278.
- WEISSMAN, I. D., BENNETT, L. H., MAXWELL, L. R., WOODS, M. W., and BURK, D., 1972. Recognition of cancer *in vivo* by nuclear magnetic resonance. *Science*, N.Y. *173*, 1288-1289.

## Book review

*Radiosterilization of Medical Products*, 1974. Pp.536, 1975 (Vienna, International Atomic Energy Agency), \$33.00.

This volume contains the proceedings of a symposium held under the auspices of the International Atomic Energy Agency at Bombay in December 1974. Of the 42 papers presented in eight sessions, the majority are in English, seven in Russian, three in French and one in Spanish.

Three sessions deal with the conditions required for the control of microbiological contamination and the dosimetric problems involved. The effects of radiation on the materials

being sterilized are considered in two sessions and an interesting final session is devoted to the types of radiation plant being used, or about to be commissioned, in different parts of the world. Also included is a report by a working party of the IAEA in which are set out revised recommendations for the radiosterilization of medical products.

This book will be useful not only for those involved in the production of sterile medical equipment, but for those wishing to obtain some background in this field.

N. E. GILLIES.